Victor S. L'vov

Wave Turbulence Under Parametric Excitation

Applications to Magnets

Springer-Verlag
Berlin Heidelberg New York
London Paris Tokyo
Hong Kong Barcelona
Budapest

8 Secondary Parametric Wave Turbulence

The present chapter deals with the non-stationary processes accompanying the parametric excitation of waves under stationary conditions when the pumping amplitude and other external parameters of the experiment are time independent. Under these conditions the system of interacting parametrically excited waves is in the flux equilibrium. Then the energy from the pumping W_+ is equal to the dissipation rate of the energy W_-: $W_+ = W_+ = W$. By the presence of the energy flux through the system the flux equilibrium differs from the thermodynamic equilibrium at which $W_+ = W_- = 0$.

The behavior of nonlinear systems in the state of the flux equilibrium is much more complicated than in the state of thermodynamic equilibrium. Thus at the thermodynamic equilibrium the average characteristics of the systems (e.g. occupation numbers) are time independent, i.e. stationary. In contrast, at the flux equilibrium as the energy flux through the system increases the stationary state under a certain $W = W_{cr}$ is no more stable. At $W \gg W_{cr}$ the behavior of these systems is usually chaotic and then their parameters (including $W(t)$) randomly depend on time. The classical examples of such systems are hydrodynamic turbulence arising when a liquid (or gas) flows past an obstacle with a large velocity and the turbulent thermal convection emerging in liquid or gas in the gravitational field and under the influence of high temperature gradients.

A nonlinear system of parametrically excited waves is not an exception. As the pumping amplitude increases (accompanied, accordingly, with the increase of the energy flux through the system) the ground state as a rule loses its stability. As a result the occupation numbers $n(\boldsymbol{k}, t)$ and phases of the pairs $\Psi(\boldsymbol{k}, t)$ at large W behave chaotically. This physical situation we shall call *secondary parametric turbulence*. The term *"turbulence"* emphasizes the similarity to the hydrodynamic turbulence. The attribute *"secondary"* points to the chaotic behavior of the already averaged (over the quasi-Gaussian ensemble of the canonical amplitudes of the waves $c(\boldsymbol{k}, t)$, $c^*(\boldsymbol{k}, t)$) quantities, i.e. double correlators $n(\boldsymbol{k}, t)$ and $\sigma(\boldsymbol{k}, t)$ of the parametrically excited waves. The secondary turbulence of the parametric spin waves has been studied in detail. It will be discussed in the following subsection.

8.1 Instability of Ground State and Auto-Oscillations

8.1.1 Properties and Nature of Spin Wave Oscillations

It is common knowledge that under parametric generation, the stationary mode often fails to be achieved and the magnetization is characterized by complicated variations with respect to some mean value. The basic experimental data on the auto-oscillations (AO) obtained for the high-quality YIG crystals under parallel pumping are as follows [8.1–3].

1. AO frequencies are within the range from 10^4 to about 10^6 Hz (depending on the pumping power p and the magnetic field H). Under small supercriticality the AO spectrum consists of a single line. As the intensity increases the number of lines also increases and they are shifted towards higher frequencies. In particular, the components emerge at multiples and at half of the frequency [8.1–3]. High above the threshold the spectrum has a noise character.

2. The AO threshold $h_{\rm cr}$ is usually very low, e.g. $0.1-1$ dB (with respect to the threshold of parametric excitations) with the exception of the range of small $k \simeq 10^3$ – 10^4 cm^{-1}, where the AO threshold notably increases. The threshold also increases when internal inhomogeneities are introduced into the crystal [8.1].

3. A giant crystallographic anisotropy of the AO is observed which significantly exceeds the anisotropy of the spin wave spectrum. Thus the AO intensity in YIG when the magnetization is oriented along the axis [111] is about 200 times as large as the intensity of these oscillations along [100].

The physical nature of AO was one of the main problems when parametric excitation of magnons is considered. Various hypotheses have been proposed. The simplest of them [8.4, 5] suggests the presence in the parametric magnon spectrum of several discrete frequencies corresponding to the eigen oscillations of the crystal. The beats between them are assumed to result in AO emergence. This hypothesis accounts well for some experimentally observed phenomena (AO dependence on the intensity and direction of the magnetic field) but completely ignores the problem of the AO frequency dependence on the pumping intensity and the origin of the various discrete frequencies. Note that the S-theory predicts the existence of only one frequency $\omega_{\rm p}/2$ in the stationary state. The other group of hypotheses is based on the assumption that parametric magnons influence the magnetization (see, for instance, study by *Green* and *Schlömann* [8.6]). If the average magnetization of the crystal follows the number of parametric magnons after a certain delay, magnetization AO can be built up in such a crystal. This viewpoint is expressed by *Monosov* in [8.1] who proceeded from the Bloch-Bloembergen phenomenological equations. Actually, however, the emergence of AO can be influenced only by the persistence of the thermal waves with the frequency of order $\omega_{\rm p}$. Therefore, the kinetic equation has to be used to study the influence of the thermal magnon persistence. It can be assumed that in most experiments the influence of the persistence can be neglected. Within the S-theory AO can be explained as a result of the instability of the stationary state described in Sec. 7.2. If at least for a single mode with m- number the instability conditions (7.1.7) are satisfied, then within the S-theory the system of parametric magnons have no stable states either. In this case there are two possibilities: either the system is pushed out of the S-theory applicability region (which is accompanied by the large amplitude increase of the excited waves) or the oscillations become steady in the stationary state. The development of these oscillations can be experimentally observed as the magnetization AO. The auto-oscillations can be expected to be, generally speaking, either regular or chaotic.

8.1.2 Numerical Simulation of Auto-Oscillation in the S-Theory

As is seen from (7.1.6) the instability of the stationary state is completely aperiodic ($\mathrm{Re}\Omega_m = 0$). Because of this it is very difficult to solve analytically the problem of the nonlinear stage of its development. Thus computer simulation seems the best way out. However, to simulate the real situation, e.g. for YIG, would take too much computer time to be practicable. Therefore a computer simulation on the simplified models of the ground state seems reasonable. In [8.3, 7] the computer simulation of the AO excitation in the "two-beam" model is described where the parametric spin waves were taken to be concentrated at two fixed angles $\Theta_1 = \pi/2$ and $\Theta_2 = \pi/4$. The coefficients $S(\boldsymbol{k}, \boldsymbol{k}')$ and $T(\boldsymbol{k}, \boldsymbol{k}')$ were chosen close to those calculated for YIG as the orientation $\boldsymbol{H} \parallel [111]$ (see below), so that the conditions of the zeroth mode instability were satisfied.

Numerical experiment showed that for such a model there is AO of the amplitudes and wave phases on the beams (Fig. 8.1). The frequency dependence of these AO on the pumping level qualitatively agrees with the similar dependence ordinarily observed in the laboratory experiment. In addition, the two-beam model is used to simulate the development of the collective instability at $m \neq 0$. The number of parametric magnons at the nonlinear stage of this instability was studied. It is an interesting problem because at the linear stage no change of the sum $(N_1 + N_2)$ takes place. The beams were chosen where $\Theta_1 = \Theta_2 = \pi/2$, $\varphi_1 = \varphi_2 = \pi/2$. The experiment showed (Fig. 8.2) that the mode is established where both the difference and the sum $(N_1 \pm N_2)$ experience oscillations. The oscillations $(N_1 + N_2)$ are due to the interaction of the collective modes with different m.

The significant result of these computer simulations consisted in the proof of the fact that at $p < p_{\rm cr1} \simeq (1.0–1.5)$ dB the system of parametric waves enters a stable limiting cycle whose field of attraction is the entire phase space. At $p > p_{\rm cr1}$ the paths near this cycle become exponentially unstable, the average divergence increment per cycle increases proportionally to $p - p_{\rm cr1}$. At small values of this difference in the vicinity of the limiting cycle a narrow layer occupied by exponentially unstable paths emerges.

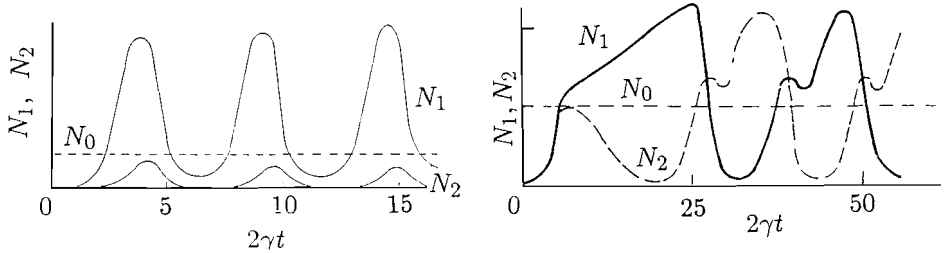

Fig. 8.1. (left) Time dependence of total numbers of pairs on beams at the instability of a zero mode. N_1 and N_2 correspond to $\Theta = \pi/2$ and $\Theta = \pi/4$; $p = 2$

Fig. 8.2. (left) Time dependence of total numbers of pairs on beams at the instability of non-zero mode. N_1 and N_2 correspond to $\phi = 0$ and $\phi = \pi/2$, $\Theta = \pi/2$, $p = 2$

The divergence of the path has been studied in a laboratory experiment by *Grankin* et al. [8.3]. They recorded the dependences $\chi''(t)$ of the different pumping pulses of one series with fixed supercriticalities and fixed other experimental conditions on one and the same screen. The only difference between successive pulses is in initial conditions at $t = 0$. At the supercriticalities $p = 2.5$ dB the successive curves $\chi''(t)$ coincide. Above this supercriticality level when the AO-Fourier spectrum undergoes a sharp broadening the curves $\chi''(t)$ for different pulses begin to diverge. At first, the divergence of nearby paths is manifested only when the time is long. Then, as the supercriticality increases, the "scattering time" becomes comparable with the AO period $\tau \simeq (3\text{–}5)/\Delta_0$ and the successive curves $\chi''(t)$ comprise a broad band.

In summary, it can be said that the computer simulation on the models reveals that within the S-theory equations the development of the internal instability of the ground state results in auto-oscillations. The properties of these AO, i.e. the dependence of the frequency and spectrum on the pumping intensity are comparable with the properties of the experimentally observed AO. In particular, under small supercriticalities both in laboratory and mathematical experiments AO prove to be periodic. An example of such a motion in the phase space is the limiting stable cycle.

In the experiments of both types the transition to the stochastic AO as the supercriticality increases takes place not via addition of new types of motion at incommensurable frequencies; it is accompanied by the broadening of the already existing spectral lines and is due to the decreasing stability of the phase paths leading to their scattering.

This implies that the secondary turbulence of spin waves arises in accordance with the concept of the strange attractor. The scenario of the route to chaos in the parametric turbulence will be treated in more detail in Sect. 8.2. For the time being discussing the rough properties of the parametric turbulence we shall only note that in computer as well as in laboratory experiments AO development does not influence significantly the

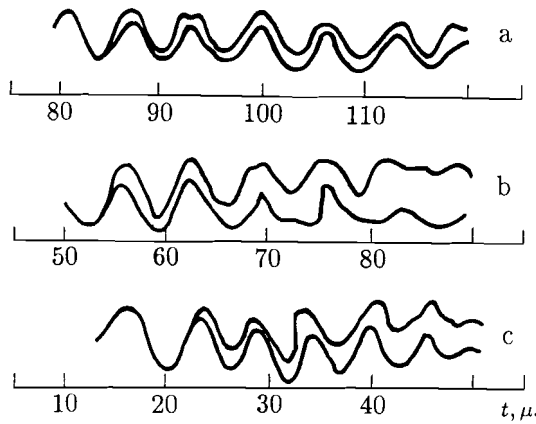

Fig. 8.3. Divergence of the trajectories $\chi''(t)$ in an experiment by *Grankin* et al. [8.3]. (a) $p = 2.6$ dB; (b) $p = 2.9$ dB; (c) $p = 3.4$ dB

average level of parametric waves. The computer simulation also shows that under the instability development the total number of parametric waves together with the observed value $\chi''(t)$ oscillate significantly at the zeroth mode and weakly when the instability is developed at higher modes. Interestingly enough, AO excitation in the computer simulation was as a rule accompanied by a decreasing average value of χ'. The same phenomenon was observed in the laboratory experiment [8.1].

8.1.3 Conditions for Excitation of Auto-Oscillations

The instability criterion (7.1.7) enables us to predict the conditions under which AO are to be observed in laboratory experiments. Let us consider the interaction amplitudes S and T for YIG calculated by *Musher*, *Starobinets* and *L'vov* by (7.1.5) for the typical experimental situation, i.e. $N = 1/3$ (sphere) $\omega_p/2\pi = 9.4$ gHz, $k = 0$ ($H = H_c$), $\omega_m = 4.9$ gHz, $\omega_a = 0.23$ gHz (room temperature). See Table 8.1

Table 8.1. Interaction amplitudes S_m and T_m for YIG (in units of $2\pi g^2$)

Orientation	T_0	S_0	$T_2 = T_{-2}$	S_2	S_{-2}
[100]	0.28	0.52	0.11	0.01	-0.36
[111]	-0.75	0.30	0.05	0.01	-1.27

As can be seen, not only the values, but also the signs of the amplitudes depend on the magnetization orientation. Substitution of the table values into the instability criterion (7.1.7) shows that in the "easy direction" [111] there is instability with respect to the zero mode, whereas in the "difficult directions" [100] all the modes in this situation are stable. Experimentally, at $H = H_c$ there are no AO in the difficult direction up to the excesses equal to (6–7) dB corresponding to the second threshold. At the same time in the

easy direction intense AO are observed practically immediately above the threshold [8.5].

The conditions of AO excitation in various experimental situations have been studied in detail by *Zautkin* and *Starobinets* [8.8]. By varying the Hamiltonian coefficients S_m, T_m within a wide range (the magnetization being varied by changing the temperature and the concentration of the admixtures as well as the shape of the sample, i.e. sphere, cylinder, disk, i.e. the direction of magnetization) they showed, in particular, that intensive AO appear only when the zeroth mode is unstable with respect to the criterion (7.1.7). At the same time the instability of the modes with $m = 0$ is always accompanied by the appearance of AO with a small amplitude (for details see Sec. 9.7). Other experimentally observed characteristic features of AO can be easily accounted for by the S-theory.

In conclusion, it must be noted that the simple AO theory described in the present section predicts that the threshold of their excitation h_{cr} coincides with the threshold of the parametric excitation h_{cr} and the AO frequency at $h = h_{cr}$ is zero. Experimentally, we observe at the same time the finite threshold of AO and the non-zero initial frequency in the YIG crystals the threshold of auto-oscillations usually equals (0.1–1) dB. The initial frequency does not correlate with the value of the threshold. Depending on the constant magnetic field it varies within the range $(10^4$–$10^5)$ Hz [8.5]. These facts can be explained by the influence of weak nonlinear damping, which does not significantly change the values χ' and χ'', by the random inhomogeneities in crystals, by the absence of exact axial symmetry, by the feedback effect on the resonator, etc. To obtain the relative contribution of those mechanisms the auto-oscillations must be further studied both theoretically and experimentally.

8.2 Route to Chaos in Dynamic Systems

We have already noted that the nonlinear system of parametric waves is an example of nonlinear dissipative systems which in the state of the flux equilibrium lose their stability as the energy flux W through the system increases. Under big W these systems are characterized by a most complicated chaotic behavior as a rule. In addition to the hydrodynamic systems, such as the atmosphere and the oceans of our planet, the chaotic behavior is characteristic of various systems in chemistry (e.g. Belousov-Zhabotinsky reactions), biology, electronics, solid-state physics, etc.

The theory of dynamic chaos as a field of theoretical mechanics and mathematics which could be applied to the above named fields has intensively developed in the last decade. Several books have been published on this topic (see, for instance, [8.9]), and the elements of this theory have already become a part of courses on theoretical physics [8.10].

A lot of interesting results were obtained when the route to chaos was studied under the parametric excitation of the spin waves [8.11–19]. This is the reason for including this section.

8.2.1 Introduction

The transition to chaotic behavior under increasing W is known to be often rather abrupt. By analogy with the radio technical generator, such excitation will be called *hard*. As a rule, the turbulence properties under hard excitation vary greatly in different systems and must be studied specifically by concrete sciences, i.e. hydrodynamic turbulence, laser physics, etc.

In other cases the route to chaos is smooth and takes place through the succession of bifurcations successively making the system's behavior more and more complex. Under small supercriticalities when the turbulence excitation is soft the number of unstable modes participating in the motion can be small, e.g. two or three. "This enables us to assume that the types of stability losses of ... the continuum could be obtained essentially in the same way as the stability analysis of the periodical movement of the dissipative discrete mechanical system described by the finite number of the equations" [8.10]. Mathematically, it means that the dimensionality of the phase space N defined as the number of the ordinary differential equations of the first order with respect to time

$$dX_j/dt = f_j(X_1, X_2, ..., X_n, t) \ , \quad j = 1, 2, 3, ..., N \tag{8.2.1}$$

describing the system is finite. Moreover, in some cases the important features of the chaotic behavior can be effectively described in the phase space of the low dimensionalities at $N \simeq 3$–5. In the limit of the small N different physical systems become more and more similar in many respects; the number of common features increases as the dimensionality of the phase space N decreases.

Let us consider as a limiting case the two-dimensional phase space concentrated on a plane. Let the phase trajectories be attracted inside a certain area and never come outside it. Since the phase trajectories do not intersect topologically they can have only three types of behavior. These trajectories are either attracted to the stationary limiting point (pole) (see Fig. 8.4A) or they are wound around it (focus) (see Fig 8.4B) or they are wound on a limiting cycle (Fig. 8.4C). In the first case the system asymptotically passes to the stationary state, in the second case the transition to the stationary state takes place through the damping oscillations, in the third case asymptotical behavior of the system is the non-damping periodic auto-oscillations. There are no other variants of behavior of the considered system.

It must be emphasized that our conclusion about the time behavior of the nonlinear system is unrelated to its physical nature. This conclusion is based only on the fact that its phase space is two-dimensional and on the

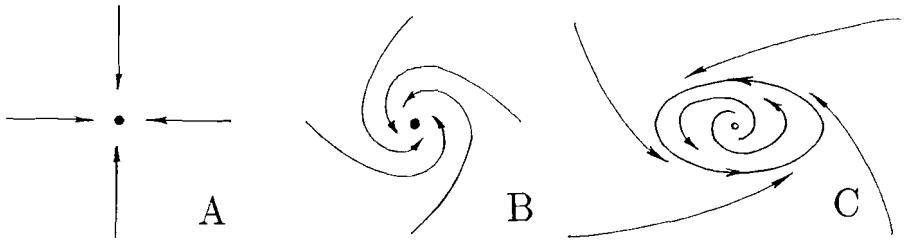

Fig. 8.4. Two-dimensional attractors: limiting point, A; stable focus, B; stable cycle, C

assumption of the presence in this space of the asymptotically attracting area, i.e. an attractor. Accordingly, experimental manifestations of a nonlinear dissipative system can help us to study the topology of its attractor on a plane, but will give us no evidence of its physical nature. Similarly, an experimental study of integers, consisting of counting apples or feeding bits of information into computers will give us no idea of the taste of apples or the physical structure of the computer memory. The different properties of integers, apples and computers are the objects of different sciences. Perhaps it is useful to know mathematics when studying apples. But will it make sense to study mathematics using only apples?

This almost absurd example can help us to understand the relation of notions in the nonlinear physics of magnets and the modern theory of the route to chaos in simple dynamic systems. Indeed, what can we learn about an antiferromagnetic $CuCl_2$ or ferromagnet $Y_3F_5O_{12}$ when we observe in them the bifurcations of doubling of the magnetization auto-oscillation periods [8.11,12]. What can be learn about the antiferromagnets $CsMnF_3$ or $(CH_3NH_3)\,CuCl_4$ if we observe in them other scenarios of the route to chaos [8.15]? Nothing, I think except the almost trivial fact that these objects are nonlinear systems of general position and thus manifest the general laws of the route to chaos.

Does this imply that the experimental study of chaos in magnets is not interesting? By no means. The mathematical theory of the route to chaos in simple dynamic systems requires not only computer studies but also physical experiments. Not, however, in order to check results like "two times two equals four" within the system of Peano's axioms, but, for example, in order to find new laws and scenarios. The universality of the laws of transition to chaos makes it possible to carry out these experiments on water and alcohol (in hydrodynamics) as well as on magnets. As in our previous example with the theory of integers and apples, the choice of the subject of inquiry is mostly a matter of personal likes and dislikes, availability and potential efficiency.

Sections 8.2.3 and 8.3.2 present an example of using the magnets as a subject of chaotization process studies. These are results of *Smirnov's* investigations of the route to chaos under the parametric turbulence of magnons

in an antiferromagnet $CsMnF_3$. This study effectively employs some notions of the dynamic chaos theory, which will be briefly described in Sec. 8.2.2.

Those readers who, first, had the patience to read my book up to this place, and, second, are not acquainted with the theory of dynamic chaos will be rewarded by the harmonic postulates of this fashionable science. In this case my task will be fulfilled. At any rate, the presented material is sufficient to form a balanced attitude to the dynamic chaos and its relative importance in the nonlinear wave theory.

8.2.2 Elementary Concepts of Theory of Dynamic Chaos

1 Landau-Hopf scenario. In order to analyze the ways of turbulence generation, let us consider phase spaces with dimensionalities larger than two which admit asymptotic motion different from a stationary point or a limit cycle. For a long time the possible attractors for a dissipative system were considered a stationary point, a limit cycle, a two- or three-dimensional torus, etc. At the n-torus the system participates with n different periods T. From this viewpoint, stationary point and the limit cycle are 0- and 1-torus. If some of the periods prove to be commensurable, the dimensionality of the torus decreases and the torus will be called a resonance torus. Thus, for instance, the trajectory on the surface of a two-dimensional resonance torus will be closed and topologically equivalent to a circle, i.e. 1-torus. In these terms, the well-known Landau-Hopf scenario of the route to chaos consists of the successive increase of the torus' dimensionality, the torus representing the system attractor. At large N the correlation functions of the system will be damped over the time of the order of T_j. However, over a very long period T_R, the so-called Poincaré recovery time, the system trajectory will pass arbitrarily close to the initial point and the correlation functions will abruptly and drastically increase up to the order of unity. The order of magnitude is

$$T_R \simeq T \exp(an)\ ,$$

where a is of the order unity.

The behavior of the nonlinear system according to the Landau-Hopf scenario seems atypical, i.e. in the space of the system parameters it can be realized over the set of zero dimension. To put it simpler, the probability of such a scenario is vanishingly small and for it to be realized special efforts are necessary, for instance $N \to \infty$ of non-interacting generators of non-commensurable frequencies should be built which will work for the common load. For more details about this scenario see Sect. 30 in [8.10].

2 Strange attractor. In 1963 *Lorenz* [8.20] considered a limitingly truncated system of equations of thermal convection in a plane layer heated from below. In a dimensionless form this system of equations is

$$dx/dt = \sigma(y - x) ,$$
$$dx/dt = -y + rx - zx , \tag{8.2.2}$$
$$dx/dt = -bz + xy ,$$

where b, r and σ are the dimensionless parameters. The phase volume of such a system decreases with time:

$$\frac{d}{dt}\text{div } \boldsymbol{R} = -(\sigma + 1 + r) < 0 , \tag{8.2.3}$$

where $\boldsymbol{R}$ is the vector x, y, z. From the Lorenz equations it follows also that

$$\frac{d}{2dt}[x^2 + y^2 + (z - r - \sigma)^2] = d(r + \sigma)^2/4 - \{\sigma x^2 + y^2 + b[z - (r + \sigma)/2]^2\} . \tag{8.2.4}$$

At large R the right-hand side is negative. This means that the distance between the points $\boldsymbol{R}$ and $\boldsymbol{R}_0 = (0, 0, \sigma + r)$ decreases with time, i.e. all the trajectories enter into some limited volume surrounding $\boldsymbol{R}_0$. Inside this volume there are no (in a certain area of changing parameters r, b and σ) stable stationary points and no stable limit cycles. As a result, phase trajectories falling into a limited volume and unable reach this stable manifold have to move in a very complicated and bizarre way. Some general considerations for the "phase portrait" for the dissipative system where the trajectories are complicated and tangled (e.g. as in [8.10]) can be given. As the system is dissipative the trajectories only enter a certain limited volume. To tangle the trajectories it is necessary that two arbitrarily close points denoting the initial conditions should move apart with time at a distance comparable with the dimensions of the attractor, i.e. *all the trajectories should be unstable*. The attracting sets of limited and unstable trajectories (the possibility of their existence has been predicted by *Lorenz* [8.20] for the case of the system (8.2.1)) are now called *strange attractors*.

Let us consider the geometrical structure in an n-dimensional space by studying the behavior of the bundle of trajectories on their way to the attractor [8.10]. In the cross-section of the bundle the trajectories fill a certain volume V in $(n - 1)$-dimensional transversal subspace. Under the motion along the trajectory the volume $V(t)$ decreases because the system is dissipative (in the conservative case V is time independent by the Liouville theorem). However, in a certain amount $m < (n - 1)$ of directions the bundle section broadens due to the exponential divergence of the unstable trajectories.

In the remaining $(n - m - 1)$ directions the bundle is compressed. The general compression must be stronger than the extension because the volume decreases. Along the trajectory the direction of compression and extension must change, or else the trajectories can fall outside the attractor. Therefore, the solid cross-section bends and at the same time flattens, bends again and

so on. This process is sometimes called *Baker's transformation* because it resembles rolling the pastry, folding it up, rolling it again, etc. The cross-section of the bundle proves to be extended and folded many times. This happens not only to the selected bundle but to any of its parts. As a result, the attractor is a system of an infinite number of flat and infinitely thin layers connected through their sides and spaced infinitely close to each other. The general volume of the attractor in its n-dimensional space equals zero. Such sets are called the Cantor sets. They are characterized by the fractional dimensionality according to *Hausdorf* $n_{\text{H}} < n$:

$$n_{\text{H}} = \lim_{\varepsilon \to 0}[\ln N(\varepsilon)/\ln(1/\varepsilon)] . \tag{8.2.5}$$

where $n(\varepsilon)$ denotes the minimum number of the n-dimensional cubes with the edge ε required for the coverage of our set. Clearly, for the part of the plane with the area S $N(\varepsilon) = S/\varepsilon^2$, therefore the limit of (8.2.5) is equal to two. For the line $n_{\text{H}} = 1$, for the set of separate points $n_{\text{H}} = 0$. For the *Lorenz* attractor $n_{\text{H}} \simeq 2.07$ (for $\sigma = 10$, $b = 8/3$, $r = 28$) [8.20]

3 Feigenbaum scenario When analyzing possible scenarios of turbulence generation under the destruction of the limit cycle it proves possible to avoid analyzing the specific type of the dynamic systems, and its general behavior can be predicted by means of the Poincaré representation. This mapping is a set of intersection points of the phase trajectory with the surface in the phase surface transverse to it. The initial dynamic system makes it possible to determine basically the intersection coordinate $\boldsymbol{R}_{n+1}$ on the $(n+1)$th round as a function of coordinate $\boldsymbol{R}_{\text{n}}$ on the previous round. In such a function of succession arises:

$$\boldsymbol{R}_{n+1} = \boldsymbol{F}(\boldsymbol{R}_{\text{n}}) . \tag{8.2.6}$$

In many cases the trajectories in the transverse subspace come very close to some line. It significantly simplifies the analysis of the trajectory behavior, because the succession function turns out to be one-dimensional

$$X_{n+1} = F(X_{\text{n}}) . \tag{8.2.7}$$

As can be easily shown (see, for instance, [8.10]), for the motion to be stochastic $F(x)$ must be a non-monotonic function. *Feigenbaum* obtained a fundamentally important result. He showed that for all the systems with one-dimensional non-monotonic mapping (8.2.7) depending on some parameter W (e.g. on the Reynolds number, pumping amplitude or on the energy flux through the system) with the extremum of the quadratic form there exists a qualitatively and quantitatively universal scenario of transition from periodic to chaotic motion, i.e. *Feigenbaum scenario* [8.21, 22].

The most important features of this scenario are shown by the mapping

$$X_{n+1} = 2CX_{\text{n}} + X_{\text{n}}^2 . \tag{8.2.8}$$

thoroughly studied, e.g. in [8.9]. The periodic motion (cycle) corresponds to the roots of the equation(8.2.8) at $X_{n+1} = X_n$. There are two such solutions

$$X_{10} = 0\ , \quad X_{11} = 1/2 - C\ . \tag{8.2.9}$$

As can be readily seen, within the range $1/2 < C < 3/2$ the cycle X_{11} is stable, and in the range $-1/2 < C < 1/2$ the other cycle X_{10} is stable. Therefore, as C decreases from $3/2$ to $1/2$, the coordinate X of the stable cycle increases from -1 to 0 and then in the range C from $1/2$ to $-1/2$ it remains equal to zero.

What happens in the range $C = -1/2 - \varepsilon$, $\varepsilon \ll 1$? In order to answer this question, periodical points of the period 2 must be considered. It can be readily obtained from the evident condition

$$X = F_2(X)\ , \quad F_2(X) = F(F(X))\ , \tag{8.2.10}$$

Here $F_2(X)$ is the square of the mapping $F(X)$, describing the mapping over two windings of the cycle

$$X_{n+1} = F_2(X_n)\ . \tag{8.2.11}$$

At $C > -1/2$ (8.2.10) has the solution (8.2.9). At $C = -1/2$ the two additional solutions appears (namely $x_{2\pm} = \pm 2$), these solutions are stable at small ε. The generation of a pair of stable points at $C < C_1 = -1/2$ describing the cycle of double period is an example of *bifurcated doubling of cycle*. As C further decreases at some $C_2 < C_1$ the double cycle is no longer stable and a new cycle with the period 4 is generated. The infinite succession of the bifurcation of the period doubling converges to the value $C_\infty = -0.78497$. At $C < C_\infty$ the motion is chaotic. *Feigenbaum* showed that at large n the succession of bifurcation values of C_H for arbitrary mapping with a single maximum has a universal behavior

$$[C_{n+1} - C_n]/[C_n - C_{n-1}] = 1/\delta \tag{8.2.12}$$

with a universal value $\delta = 4.6692$ [8.22].

4 Reciprocal bifurcations of chaotic motion. In the previous subsection we gave a brief description of the succession of period doubling bifurcations for the mapping (8.2.8) with C changing from $C_1 = -1/2$ to $C_\infty = -0.78497$. What is the nature of motion for $C < C_\infty$?

This range has been studied by *Lorenz* [8.23], *Collet* and *Eckmann* [8.24] and *Helleman* [8.25]. In computer experiments they observed that as C decreases the bands of chaotic motion merge and experience inverse bifurcations at some points $C = C_n$. It was also found that bifurcations of the limit cycles with the period $n = 6$, 5 and 3 cutting the chaotic area. The reciprocal bifurcations of the chaotic bands obey the similarity law (8.2.12) with the same constant [8.26].

5 Pomeau-Manneville scenario The quadratic mapping of the form

$$X_{n+1} = X_n^2 + X_n + \varepsilon \tag{8.2.13}$$

demonstrate one more kind of bifurcation, i.e. the so-called reciprocal tangential bifurcation [8.27]. As values change from negative to positive the stable and anstable points of this mapping merge and vanish [8.28]. This bifurcation is characterized by another type of route to chaos-via intermittence. It is usually called the *scenario of Pomeau-Manneville*. In this case the ranges of almost chaotic motion are chaotically overlapped by the successive ranges of irregular motion. The average length of coherent beams decreases as $1/\sqrt{\varepsilon}$. Interestingly, the route to chaos in the system (8.2.8) from the integer cycles corresponding to the value $C < C_\infty$ when the C parameters increases (and not decreases) takes place in accordance with the scenario of Pomeau-Manneville without period doubling.

In conclusion it must be emphasized again that the survey of the scenario of the route to chaos in this section is by no means exhaustive or complete. My intention was to give the reader the most important mapping used in the interpretation of experiments on chaos in magnets [8.11–19], and I mostly followed the textbook [8.10] and *Smirnov*'s doctorate thesis [8.28].

8.2.3 Chaos of Parametric Magnons in $CsMnF_3$

In recent studies of parametric secondary turbulence [8.11–19] this problem was connected with the modern ideas of chaotic dynamics of nonlinear dissipative systems. The first observation of a complete doubling route to chaos was made by *Gibson* and *Jeffries* [8.12] with the second-order Suhl process in a Ga-YIG. *Waldener, Barberis* and *Yamazaki* [8.13] observed a route to chaos by irregular periods, and *Yamazaki* [8.11] observed one period doubling but no chaos in AFM $CuCl_2$. The first observation of subharmonic routes to chaos was made by *Resende* et al. in 1986 in pure YIG spheres. A detailed review of experimental studies of chaos origin in magnetic systems is given in [8.17, 19]. In this section we shall consider only *Smirnov's* results concerning the antiferromagnet $CsMnF_3$ as an example of an advanced experimental study of this problem.

1 Main results. In [8.16] the time dependence of the power $W(t)$ absorbed by the sample of $CsMnF_3$ was studied under different amplitudes of pumping h and varying values of the external magnetic field H. Depending on the values of $p = h^2/h_{th}^2$ different modes of $W(t)$ behavior were observed (see Fig. 8.5 [8.16]). These include stationary state $W(t)$ (mode 0), periodic autooscillations of the relaxation character with the period $t \simeq 0.1$ ms mode 1. The bifurcations of doubling and quadrupling of the period of the basic motion, modes 2 and 4, were also observed as well as the cycles with periods $3T$, $5T$ and $7T$, modes 3, 5, 7. The mode of chaotic motion was observed

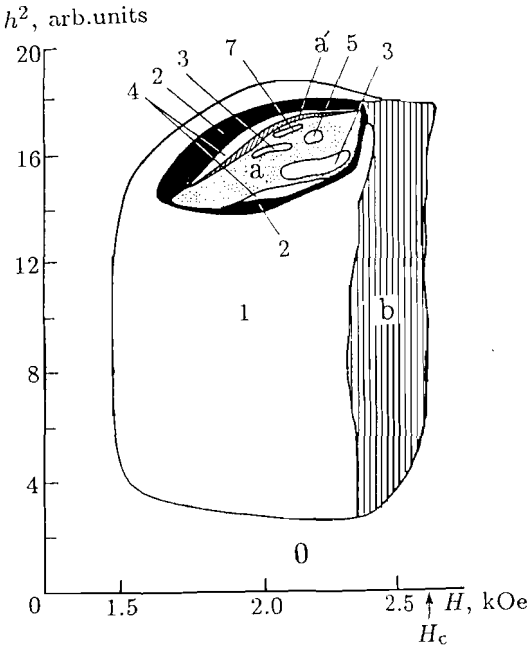

Fig. 8.5. Diagram of stationary (0), periodic (1) – (7) and chaotic (a,a' and b) regimes. Periodic situations of the corresponding multiplicity (from 1 to 7); a-chaos 1 (motion in one and two zones); a'-chaos 1 (motion in four zones); b-chaos 2.(after *Smirnov* [8.16]

whose spectrum contains merged lines at the frequencies $f = 1/T$, $1/2T$ and $1/4T$ which was called Chaos 1, and another type of chaotic motion with a wide spectrum called Chaos 2. The diagrams in Fig. 8.5 shows the general succession of bifurcations leading to changing of the modes. Fig. 8.6 shows the cross-section of this diagram (with higher resolution of p) in the field $H = 2.0$ kOe. Following [8.16], let us treat this cross-section in more detail.

2 Fine structure of the mode change of AO depending on pumping intensity. As can be seen from Fig. 8.5, the transition from the periodic mode of auto-oscillations of the absorbed power to "chaos 1" takes place in compliance with the Feigenbaum scenario, i.e. through period doubling. As described in Sec. 8.2.2, the analysis of the quadratic mapping (8.2.8) made it possible to clarify many other details of mode change under changing C parameter which, as it turned out, appear in experiment [8.16]. Fig. 8.6 shows the temporal sequence of the different types of microwave absorption observed in the field of 2.0 kOe when the pumping power was varied. Most consistently the Feigenbaum scenario and other details of the mode change typical of the mapping (8.2.8) are manifested as the intensity changes from high to low values. The process of the inverse bifurcation of doubling - the merge of external zones of the phase-plane diagram is clearly seen. The spectra of chaotic motion at the parameter values corresponding to these transitions must have a form universal for many systems [8.29] (see [8.9], Fig. 7.23). The spectrum obtained for the value $C = C_2$ corresponding to the merging

of the four zones into two has a sharp peak at the frequencies $f/4$ and $f/2$ and broad peaks of lower amplitude at the same frequencies. The wide and sharp peaks at the frequency $f/2$ are characteristic of $C = C_1$ (two zones merge into one). These spectra qualitatively agree with the spectra experimentally observed in [8.16].

The laws of transition from the loop modes with periods 7 ,5, 3 to the chaotic modes are of considerable interest. In the experiment [8.16] the transient (from cyclic to developed chaotic period) was observed only for the cycle with the period 3. As the power decreases the period is doubled, i.e. a cycle with period 6 is generated. The exit from the cycle 3 in the opposite direction (as the power increases) takes place in a different way. The spectral lines corresponding to the cycle 3 rapidly broaden and the real signal reveals the intermittence of wave packets from the cycles 3 and chaotic intervals. Unfortunately, in experiment [8.16] the intermittence was observed in a very narrow intensity range, so that it is not possible to obtain the power dependence of average duration of coherent wave packets. However, it can be positively assumed that in this experiment intermittence is due to the merge and vanishing of stable and unstable cycles, since the place of this mode change is determined by all the remain bifurcations.

Following *Lorenz* [8.9] a dependence $y_{n+1}(y_n)$ for the chaotic mode (position 8, Fig. 8.6) can be plotted where y_n is the absolute value of the n-th minimum on the $W(t)$ dependence. Such a plot determines the Poincaré mapping for the surface parameterized by the condition of the maximum of this coordinate in the phase space. The plot of this dependence is shown in Fig 8.7A and has the form of a curve with the minimum. According to Feigenbaum's theory, the system with such Poincaré mapping during the transition to chaos must experience a cascade of duplication bifurcations. This implies [8.9] that close phase trajectories diverge exponentially with time, and that the attractor of our system is strange one. The construction of mapping y_{n+1} (y_n) for the chaotic mode near the intermittence of the cycle 3 and also for "chaos 2" brings about no unambiguous dependence (Fig. 8.7B). The same situation with mapping is evidently also observed in the numerical experiment on the mapping (8.2.8), and the C value close to the value under which cycle 3 arises at the approach from the condensation point of duplication bifurcations (see [8.9] and Fig. 15 in [8.9]).

Note also that the transition from the mode of chaotic motion corresponding to the position 12 on Fig. 8.6 to the mode of the position 13 is accompanied by a small hysteresis and is usually associated with the two chaotic attractors of the system in this range of the parameter values.

A close observation of the transition from the cyclical mode of the fundamental cycle to "chaos 2" revealed that this transition also takes place through intermittence. Experiment shows that the mean value $\langle 1/\tau \rangle$ (τ is the duration of coherent wave packets) depends on $\varepsilon = (H - H_{cr})$ as ε^2 (see [8.16], Fig. 11). The "chaos 1" is characterized by the order close in time,

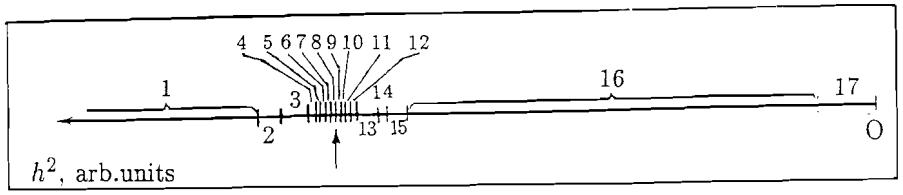

Fig. 8.6. Sequence of transformation of periodic and chaotic regimes in a field of 2.0 kOe as the power is varied. (1)-steady state; (2)-cycle of fundamental period; (3)-cycle 2; (4)-cycle 4; (5)-chaos of four zones; (6)-chaos of two zones; (7)-cycle; (8)-chaos of one zone; (9)-cycle 3; (10)-cycle $6 = 3 \times 2$; (11)-chaos of one zone; (12)-zone contraction; (13)-chaos of one narrow zone; (14)-cycle 4; (15)-cycle 2; (16)-cycle of the fundamental period; (17)-steady state. The arrow points to the value of h^2 at which the intermittency of cycle 3 is observed

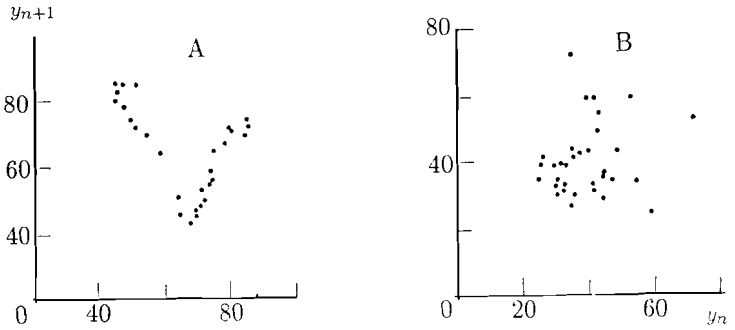

Fig. 8.7. (A) Poincaré mapping for chaotic regime 8 in Fig. 8.6, (B) for chaos (after [8.16])

which is confirmed by the observed dependence $y_{n+1}(y_n)$ (Fig. 8.7A) and also a fixed hierarchy of the mode transformations under intensity changes (Fig. 8.6).

In conclusion, we can say that in the discussed example of the secondary turbulence in the antiferromagnet $CsMnF_3$ the route to chaos follows the Feigenbaum scenario (through period duplication) if the pumping intensity is increased under an increasing magnetic field. The Pomeau-Manneville scenario is set (transition through the intermittence of coherent wave packets). Many details of the evolution of the time, spectral and amplitude motions of the system of parametric magnons are observed, theoretically predicted on the basis of the quadratic mapping (8.2.8), i.e., periodic motion with the period multiple of 3,5,7, bifurcation of the cycle 3 intermittence, merging of chaotic zones.

8.3 Geometry of Attractors of Secondary Parametric Turbulence of Magnons

8.3.1 Effective Phase Space and Dimensionality of Inclusion

As has already been noted, the modern approach to the problem of turbulence generation is based on the assumption of the finite dimensionality of the phenomena which determine the development of instabilities. Although the rigorous mathematical formulation of this statement, i.e. the theorem of central variety [8.30] has been proved only for the bifurcation of stability loss of the stationary point, there are intuitive arguments [8.10] in favor of the existence of a finite set of essential modes or degrees of freedom which determine the system dynamics over a long time and for more complicated modes of motion.

In this respect it is interesting to obtain experimentally the number of independent variables unambiguously describing the potentially infinite dimensional motion of the dissipative continuum system when the number of degrees of freedom really involved in motion is not known beforehand. To define the necessary number of such variables will mean to construct one-to-one mapping of the phase space of the asymptotic motion mode onto the Euclidean space of these variables; therefore this number can naturally be called the dimensionality of inclusion n_e [8.31-33].

The first attempts to construct an infinite dimensional phase space on the basis of measurement results were associated with the simultaneous measurements of a number of independent quantities in hydrodynamics [8.33, 34]. The next important step was to prove the fact that the phase coordinates $X_j(t)$ for time t may can be taken in the form $X_j(t) = a[t + (i-1)T]$, where $a(t)$ is the only measurable quantity and T is the shift in time [8.31, 32]. For the position P of the mapping points on the trajectory in the equivalent phase space to be in one-to-one correspondence with its position in the real phase space of the system the number of variables X_j must be not less than $(2n_H + 1)$ where n_H is the dimensionality of the attractor according to Hausdorf in the real phase space [8.32]. In cases when the attractor's geometry is simple and its mappings onto the space of the equivalent variables have no self-cross sections, the number n_e can be decreased down to n_H. In [8.32] – a fundamental research for this analysis – this procedure was shown to obtain the correct topology of the attractor as well as to enable one to accurately determine the values of all the Lyapunov exponents. The physical meaning of this procedure consists in the fact that the values of one variable (called T) are determined by the interaction with all the essential variables of the problem. Therefore the evolution history of this variable $a(t)$ contains (in indirect form) the information about the values of other variables in previous times.

In order to determine the n coordinates $X_j(t)$ of the point in the equivalent phase space measurements of the value of one coordinate $a(t)$ over n

times are used, i.e. the data are not taken from nowhere as it may seem. The experimenters must find very attractive such a construction algorithm of phase space of any dimensionality by means of measuring the time dependence of only one value, because they always have time but not always the chance to put any amount of sensors on the object of their observation.

If the number of important variables n_e is not known beforehand (as is usual in the case of distributed systems) it must also be found from the experiment how many coordinates describe the evolution of the system. We could employ here a convenient geometric criterion formulated in [8.33], it is equivalent to the distribution criterion of the joint probability [8.31]. If $n > n_e$, then any measurable quantity $y(X)$ must be a function of the constructed n-phase variables $y(X) = f(X_1, X_2, ..X_n)$. If $n < n_e$, then in the general case y will not be a function of $X_1 ... X_n$, than y should be added as a $n+1$ coordinate. Therefore, beginning with coordinate $n = 1$ it is necessary to add new coordinates one by one and to check for the functional dependence on the previous coordinates. Under the moving point $\boldsymbol{X}(t)$ the repetition of the vector $\boldsymbol{X}$ results in the repetition of $\boldsymbol{y}$ if there is a functional dependence and brings about no such repetition if there is no such dependence. This circumstance is conveniently checked graphically. To this end we plot as abscissa the distance $r_n^2 = \sum_{j=1}^{n}(X_j(t) - X_j^0)^2$ from the current position of the point on the attractor to some fixed point $\boldsymbol{x}^0$ on this attractor. On the y-axis we plot the value $d = |\boldsymbol{X}_{n+1}(t) - X_{n+1}^0|$. If the above described functional dependence exists, then $d \to 0$ at $r_n \to 0$. Let us call this check of the functional dependence the *criterion* 1. To realize this criterion in an n-dimensional sphere with a small radius there must be only a few points on the attractor unlike the methods which determine Hausdorf's dimensionality of the attractor. The authors of [8.33] formulated another less exact criterion (let us call it *criterion* 2) which excludes all the small scales. According to the criterion 2 the dimensionality n_e is achieved if the envelope of the trajectory on the plane r,d is completely below the straight line $d = Kr$ where $K \simeq 1$. The criterion 2 can be varied usefully for large dimensionalities of inclusion when the number of the experimental points on the attractor in the volume limited by small linear dimensions is small. The dimensionality n_e obtained by the criteria 1 and 2 in some specific cases can be decreased, for instance, by means of additional cross-sections, as will be described below, or by using the rotated coordinate system.

8.3.2 Experimental Study of Attractor Structure in $CsMnF_3$

In the present section we shall dwell further on the interesting results obtained by *Smirnov* [8.6] in his research on the secondary parametric turbulence of magnons in $CsMnF_3$. Fig. 8.8 shows projections of attractors onto the plane $W(t)$, $W(t+T)$ taken from this work. Modes (1), (2), (3) on this figure correspond to the "chaos 1" on the diagram on Fig. 8.5 and to the

modes (5), (8), (11) on Fig. 8.6. The modes (4) and (5) on Fig. 8.8 correspond to "chaos 2" on the mode diagram. The mode (4) is transient from the cycle of the basic period to "chaos 2".

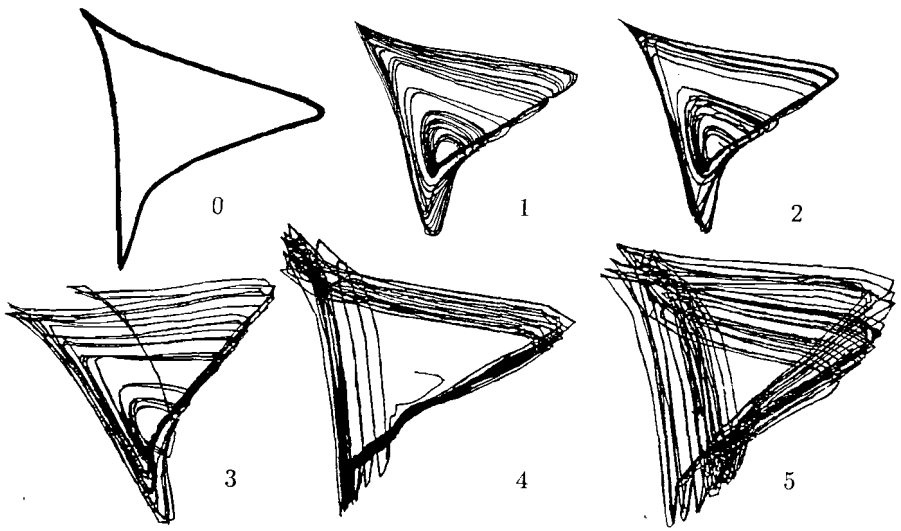

Fig. 8.8. Phase portraits for the periodic (0) and chaotic regimes (1-5) (following [8.17])

Constructing the trajectory on the plane r_n,d we obtain by the criteria the following dimensions of inclusion: for modes (1), (2), (3) $n_e = 3$, in the mode (4) $n_e = 3$, for mode (5) - $n_e = 5$ by criterion 1 and by criterion 2.

The shape of the attractors included into the 3-dimensional space can be studied in detail by means of plane cross-sections. The points where the phase trajectory crosses the intersecting plane are located on line segments, i.e. the attractor is formed from a two-dimensional band which at the intersection with cross-secting planes form the line segments. These plane bands form foldings as well as the branches in the band planes, and afterwards the branch is imposed on the main part of the band.

By constructing a number of cross-sections we can obtain an unambiguously topological structure of the attractor for each of the modes (1), (2), (3), Fig. 8.9 shows the topological equivalents of these attractors.

For the mode (1) the attractor is topologically equivalent to the Rössler attractors [8.9] for those parameter values under which the motion takes place in two zones, i.e. it is a two-loop spiral from a flat band with folds (see Fig. 55 [8.9]) In the Rössler attractor under its evolution towards the increase of the area of chaotic change of variables the foldings are embedded into each other, which results in the loop been formed from a plane strip of the flat band with a fold. The chaotization of the motion in this case occurs at the expense of the divergence of the trajectories in the band

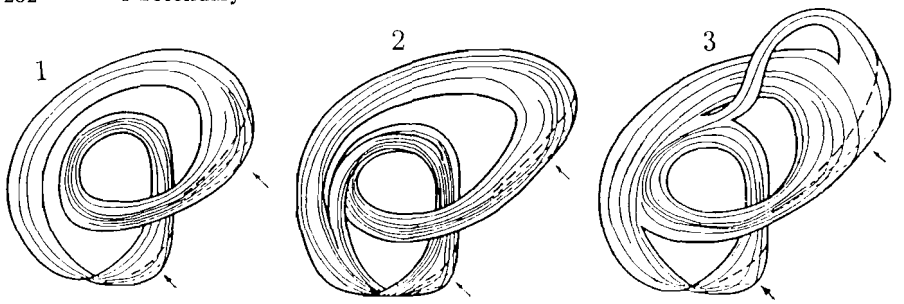

Fig. 8.9. Topological equivalents of the attractors for the regimes 1-3. The arrows indicate the folds

plane and their missing as a result of folding (the above named Baker's transformation).

A spin-wave turbulence attractor develops in a different way. In the transition to mode (2) a small strip branches off the plane, departs from the large loop und is superposed on the trajectory of the small loop as the planes graduallally converge. Such a chaotization of trajectories takes place in the *Lorenz* attractor.

In the attractor of the mode (3) the edges of the band merge at the small and large loops and the branching-off belt of the Lorenz attractor type passes over from the internal orbits to the external orbits making there one more folding.

Therefore, the attractors for the modes corresponding to the "chaos 1" can be constructed from the elements of the Rössler and Lorenz attractors. They correspond to the motion with the least state of chaos in the sense that the phase trajectories in them diverge in one direction only (they have only one positive Lyapunov exponent).

The described cross-sections also reveal the traces of the fractal structure of the attractor, i.e. in the layer which can be called two-dimensional with some finite accuracy there turns out to be one more layer than the resolution scale, which in turn, must also consist of layers, etc. Thus it can be seen on the cross section 5 that the attractor band giving a branch of the cross-section inclined to the vertical axis of the figure of about 45° is layered.

For modes (4) and (5), the cross-section (Fig. 4 in [8.16b]) show that the projections of the corresponding attractors in the three-dimensional space are solid: the points where the trajectories pierce the cross-section planes fill the two-dimensional sections. Therefore, the trajectories in mode (4) mix in the solid tube of the trajectories (convergence takes place in two directions, and the dimensionality of the flux is not less than 4) and for mode (5) the trajectories miss in the space of still larger dimensionality, although its dimensionality is limited and does not exceed 5.

In conclusion I should like to emphasize that the information on the dimensionality of the attractors of different dynamic system is undoubtedly necessary for the study of their statistical behavior. This, however, is only a small part of the information required. Again I should like to bring an analogy. Both dogs and chairs have four legs unlike the three-legged pianos and two-legged ostriches. Does this imply that the statistical behavior of dogs and chairs is similar and ostriches resemble pianos more than dogs? By no means. But, on the other hand, the information about the number of legs is not useless. Thus, a three-legged chair will fall more often and a dog devoid of one leg will also behave strangely. Similarly, the information about the attractor dimensionality is interesting not only from the geometrical, but also from general point of view. It is necessary, for instance, when seeking equations simpler than the input equation that determine the behavior of the dynamic systems in the range of supercriticalities where the dimensionality of the attractor is significantly less than the dimensionality of the phase space.

8.4 Secondary Turbulence and Collapses in Narrow Parametric Wave Packets

Throughout this book the threshold of the parametric instability has been assumed to be minimum for the wave pairs with vectors $\pm\boldsymbol{k}$ filling line or surface in $\boldsymbol{k}$-space. The phase sum in the pair is in this case a dynamic variable and individual wave phases are chaotic with a good accuracy. Now we shall describe the situation when the excitation threshold is minimum for the only pair $\pm\boldsymbol{k}_0$, e.g. under parallel pumping in uniaxial ferromagnets with the anisotropy of the "easy-plane" type. The basic peculiarity of the problem is the narrowness (in each direction) of the wave packets excited in the $\boldsymbol{k}$-space. On the one hand, in this case we cannot employ the statistical description as in the S-theory, on the other hand, this enables us to reduce the interaction Hamiltonian using other parameters, i.e. the narrowness of the packet. To this end, the problem must be formulated in terms of complex amplitudes of the envelopes of the waves.

8.4.1 Equations for Envelopes

By using the canonical equations of motion with the exact Hamiltonian $\mathcal{H}_{\text{int}} = \mathcal{H}_{\text{p}} + \mathcal{H}_4$ given by (5.2.1) and (1.1.32) and assuming that then in the $\boldsymbol{k}$-space narrow wave packets are excited

$$a(\boldsymbol{k}) = [A(\boldsymbol{k} - \boldsymbol{k}_0) + B(\boldsymbol{k} + \boldsymbol{k}_0)]$$

we also obtain, as in Sec.4.1., the equations for the complex amplitudes of the envelopes $A(\boldsymbol{r}, t)$, $B(\boldsymbol{r}, t)$. These are the Fourier components of $A(\boldsymbol{\kappa}, t)$ and $B(\boldsymbol{\kappa}, t)$. The resulting equation has the form

$$\Big[i\Big(\frac{\partial}{\partial t}+\boldsymbol{v}\cdot\nabla\Big)+\frac{1}{2}\hat{L}\Big]A(\boldsymbol{r},t)=-i\gamma A(\boldsymbol{r},t)+hVB^*(\boldsymbol{r},t)+$$
$$+\big[\omega(\boldsymbol{k}_0)-\frac{\omega_\mathrm{p}}{2}+T|A(\boldsymbol{r},t)|^2+2S|B(\boldsymbol{r},t)|^2\big]A(\boldsymbol{r},t)\ ,$$
$$\Big[i\Big(\frac{\partial}{\partial t}+\boldsymbol{v}\nabla\Big)+\frac{1}{2}\hat{L}\Big]B(\boldsymbol{r},t)=-i\gamma A(\boldsymbol{r},t)+hVA^*(\boldsymbol{r},t)+ \tag{8.4.1}$$
$$+\big[\omega(\boldsymbol{k}_0)-\omega_\mathrm{p}/2+T|B(\boldsymbol{r},t)|^2+2S|A(\boldsymbol{r},t)|^2\big]B(\boldsymbol{r},t)\ ,$$

where

$$\boldsymbol{v}=\frac{\partial\omega}{\partial\boldsymbol{k}}\ ,\quad \hat{L}=\sum_{i,j}\frac{\partial^2\omega}{\partial k_i\partial k_j}\frac{\partial^2}{\partial x_i\partial x_j}\ ,$$

$$T=T(\boldsymbol{k}_0,\boldsymbol{k}_0;\boldsymbol{k}_0,\boldsymbol{k}_0)/2\ ,\quad S=T(\boldsymbol{k}_0,-\boldsymbol{k}_0;\boldsymbol{k}_0,-\boldsymbol{k}_0)/2$$

(the amplitudes of wave interaction). Equations (8.4.1) have a trivial solution

$$A(\boldsymbol{r})=|A_0|\exp(-i\Psi_1)\ ,\quad B(\boldsymbol{r})|A_0|\exp(-i\Psi_2)\ ,$$
$$2|S|A_0^2=\sqrt{(hV)^2-\gamma^2}\ ,\quad \sin(\Psi_1+\Psi_2)=\gamma/hV\ , \tag{8.4.2}$$
$$\Psi_1=\Psi_2=\Phi/2\ ,$$

corresponding to the excitation of a standing wave $\pm\boldsymbol{k}_0$. I showed [8.35] that the solution (8.4.2) is practically always unstable with respect to increasing valuation of amplitudes and phases of envelope waves

$$\delta A(\boldsymbol{r},t)\propto\exp(i\boldsymbol{\kappa r}+\nu(\boldsymbol{\kappa})t)\ ,\quad \delta B(\boldsymbol{r},t)\propto\exp(i\boldsymbol{\kappa r}+\nu(\boldsymbol{\kappa})t)\ .$$

The development of the instability significantly depends on the amplitudes of the interaction Hamiltonian. With the exception of the case $T>0$, $S>0$, which will not be discussed the instability increment is maximum on the surface $\boldsymbol{\kappa}\perp\boldsymbol{k}$ and has the form [8.35]:

$$[\gamma+\nu(\kappa)]^2-\gamma^2=\begin{cases}-\frac{1}{4}\hat{L}\kappa^2(\hat{L}\kappa^2+4TA_0^2\\ -8S(2S+T)A_0^4-\frac{1}{4}\hat{L}\kappa^2(\hat{L}\kappa^2+4(4S+T)A_0^2.\end{cases} \tag{8.4.3}$$

At the distance from the surface it decreases rapidly. Because of this the main properties of the nonlinear stage of the instability can be described by means of the two-dimensional equations (8.4.1) where A and B depend only on the coordinates x and y orthogonal to $\boldsymbol{v}$. The upper and lower lines in the expression (8.4.3) correspond to perturbations of the type $\delta A(\boldsymbol{r},T)=\pm\delta B(\boldsymbol{r},t)$. When $T>0$, $S>0$ the perturbation of the type $\delta A=-\delta B$ is seen to have a reserve of stability. As shown in [8.35], the relation $A(\boldsymbol{r},t)=B(\boldsymbol{r},t)$ is also valid on the nonlinear stage of motion. Limiting ourselves for simplicity by the case $\omega''>0$ we can reduce (8.4.1) by changing the scale

$$i\Big(\frac{\partial}{\partial t}+\gamma\Big)A-hVA^*+\frac{1}{2}\Delta A=[(2S+T)|A|^2-TA_0^2]A\ . \tag{8.4.4}$$

Here we determined $\omega(\boldsymbol{k}_0)$ by the condition of external stability. Thus the most stable standing wave is selected for which, as shown in [8.35], the area of the positive increment in the $\boldsymbol{k}$-space is limited: $\nu(\kappa)>0$ at $\kappa<\kappa_\mathrm{c}$ where $\kappa_\mathrm{c}\ll k_0$. The nonlinear instability stage of the plane standing wave for the further development will be studied within the scope of (8.4.4) formulated here.

8.4.2 Stationary Solitons

The simplest variant of nonlinear behavior of the system is its transition to the stationary state different from the plane standing wave $A=\mathrm{const}$. Therefore in this section we shall consider the stationary solutions of the basic equations (8.4.4). As a rule, these solutions are deep non-sinusoidal variations of the amplitude $A(\boldsymbol{r})$ and phase $\Phi(\boldsymbol{r})$ and they can naturally be called *solitons*.

The solitons with a constant phase $\Phi(\boldsymbol{r})=\Phi_0$ can be studied most conveniently. It follows from (8.4.4) that

$$hV\sin\Phi_0=\gamma\ ,$$

and for $C=|A(\boldsymbol{r})|$ we have the equation

$$\Delta C=C[hV\cos\Phi_0-TC_0^2/2+FC^2]\ . \tag{8.4.5}$$

where C_0 must be understood as the initial amplitude of the pair. Taking into account that $hV\cos\Phi_0+SC_0^2=0$ let us write (8.4.5) as

$$\Delta C=-dU/dC\ . \tag{8.4.6}$$

For the plane solitons $C(x)$ this equation describes the motion of the nonlinear oscillator with the coordinate C in the potential field $U(C)=FC^2(2C_0^2-C^2)/8$ where x acts as time. The behavior of the solution is characterized by the "energy" of the oscillator. The case $F>0$ is the most interesting because in this case there exist solutions with a little difference from the plane wave. They are realized at E close to $E_\mathrm{min}=FC_0^2/8$ and are weakly modulated plane wave $C(x)=C_0-C_1\cos\kappa_0 x$, where $\kappa_0^2=-FC_0^2$. Such solutions ($C_\perp\ll C_0$) we shall call *small solitons*. As the energy increases the amplitude and the oscillation period increase. At $E=0$

$$C(x)=2\sqrt{C_0}/\cosh(x\kappa_0/\sqrt{2}) \tag{8.4.7}$$

and passes to the solitary wave, i.e. the *single soliton* which is the analogue of the plane self-focusing beam in the nonlinear medium. At $E>0$ the solution resumes its periodic structure, but now it changes within the limits symmetrical about zero. Small solitons with the variable phase

$$\Phi(\boldsymbol{r})=\Phi_0+\Phi_1\cos\boldsymbol{\kappa r}\ ,\quad C(\boldsymbol{r})=C_0+C_1\cos\boldsymbol{\kappa r} \tag{8.4.8}$$

have the size

$$|\kappa|^2 = |\kappa_1|^2 = -2SC_0^2 \ , \quad \gamma\Phi_1 = TC_0C_1 \ . \tag{8.4.9}$$

We draw attention once more to the evident fact that the characteristic dimensions κ_0 and κ_1 of the small solitons correspond to those κ for which the increment of the plane wave described in [8.35] becomes zero:

$$(\nu+\gamma)^2 - \gamma^2 = \frac{1}{2}(\kappa^2 - \kappa_0^2)(\kappa^2 - \kappa_1^2) \ , \quad \kappa_0^2 = -(2S+T)C_0^2 \ .$$

When studying very deep solitons with a variable phase when in (8.4.4) the damping and pumping can be neglected we again come to (8.4.6) with the potential

$$U = -FA^4/8 + \alpha^2/2A^2 \ , \tag{8.4.10}$$

where α is an arbitrary constant. There are also deep solitons moving with a constant velocity. In this case the term $v^2C^2/8$ is added to the potential of the deep solitons.

The analysis performed by *L'vov* and *Rubenchik* [8.36] enables us to assume that all the stationary solitons in (8.4.4) are unstable. In the same work the initial nonlinear stage of this instability was treated and special attention was paid to the case when the increment was abnormally small.

Interestingly, the nonlinear interaction becomes significant at very small amplitudes. Nevertheless, it does not lead to the limitation of the amplitudes. There is only a decrease in the rate at which the initial perturbation grows thus slowing it down significantly. In this case the amplitude increases as $\sqrt{t}$. A narrow in the $\boldsymbol{k}$-space wave packet is generated ($\kappa \sim \kappa_0 \ll k_0$, $\Delta\kappa \sim \kappa_0$). Such a state is highly turbulent and will be studied in the next section.

8.4.3 Average Characteristics of Secondary Turbulence

First, let us estimate the width of the area excited in the $\boldsymbol{k}$-space at arbitrary supercriticality. It follows from the basic S-theory that in the case under discussion when $V(\boldsymbol{k})$ has its maximum at the point $\boldsymbol{k}_0$ the packet of parametrically excited waves relaxes to the standing monochromatic wave with $\boldsymbol{k} = \boldsymbol{k}_0$ if the individual wave phases can be considered random. It is sufficient for the phase randomness that the phases of two waves in a packet have to diverge at a value of about unity over the time less than the characteristic time of the nonlinear interaction. This takes place in a packet with $(\Delta k)^2 \gg \kappa_0^2 = SA_0^2/\omega''(\boldsymbol{k})$. Therefore the packet with $\Delta k \gg \kappa_0$ narrows up to the size $\sim \kappa_0$ and its mean amplitude relaxes to the value $\sim A_0$. But if $\Delta k \ll \kappa_0$, then such a packet is unstable with the increment (8.4.3) with respect to the perturbations with $\kappa \sim \kappa_0$ and, consequently, will broaden

up to $\Delta k \sim \kappa_0 \sim \sqrt{SA_0^2/\omega''}$. Note that in the whole area of the turbulent motion the instability increment (8.4.3) is positive in the narrow layer $\kappa v \le SA_0^2$ close to the plane $\boldsymbol{\kappa} \perp \boldsymbol{v}$. So the turbulence considered is almost two-dimensional, namely:

$$(\kappa_\parallel/\kappa_\perp)^2 \sim SA_0^2/\omega(k) \ll 1 \ . \tag{8.4.11}$$

The mean level of turbulence A^2 cannot differ greatly from A_0^2 given by the (8.4.2). Indeed, as has already been noted, it was shown in [8.35] that the monochromatic plane wave is stable with respect to the short wave perturbations with $\kappa \simeq k_0$ only if the amplitude equals to A_0. Evidently, such instability is retained also for the pair modulated with $\kappa \ll k_0$. So if A_0^2 differs appreciably from A^2, short wave modulations are excited, which contradicts the above-found narrowness of the packet. Therefore, the instability development of the plane wave leads to a strong quasi-two-dimensional wave turbulence of the modulation $A(\boldsymbol{r}, t)$ with a mean level

$$\langle A^2 \rangle \simeq \langle A_0^2 \rangle = \sqrt{h^2V^2 - \gamma^2}/2S \ , \tag{8.4.12}$$

and with the modulation depth of the order unity, characteristic frequency of motion $(hV - \gamma)$ and with the characteristic scale in the coordinate space $r_\perp \sim \kappa_0^{-1} > k_0^{-1}\sqrt{\omega(k)/2A_0^2}$. We can say that there arises a dynamic soliton structure with the coherence length of the order of the soliton size, i.e. $\sqrt{\omega''/S}/A_0$ which changes significantly in space over a time $1/(hV - \gamma)$.

8.4.4 Destruction of Parametric Solitons with Large Amplitude

In the areas where the soliton amplitude during the turbulent motion proved to be anomalously large $A \gg A_0$ damping and pumping in the equations of motion can be neglected, because over the characteristic time of the problem $1/SA^2$ the system will not have enough time for significant energy exchange with the thermal bath and pumping. In this approximation (8.4.1) describe the non-stationary behavior of wave pair in a conservative medium. The behavior of one almost monochromatic wave in the nonlinear medium has been experimentally and theoretically studied using computers in association with the problems of nonlinear optics [8.37], plasma and hydrodynamics [8.38, 39]. The phenomenon of light self-focusing was discovered [8.40]. Later it was shown that the self-focused light beam is unstable, in some cases this instability leads to the short-time collapse of the beam [8.41, 42].

It will be shown below that similar phenomena take place also in our case of the wave pair. The direct calculation can show that (8.4.1) have the following integral of motion:

$$\begin{aligned} I = &\frac{\omega''}{2}\int(|\nabla B|^2)\,d\boldsymbol{r} + \\ &+ \frac{T}{2}\int(|A|^4 + |B|^4)\,d\boldsymbol{r} + 2S\int |A|^2|B|^2\,d\boldsymbol{r} \ . \end{aligned} \tag{8.4.13}$$

Let us show that its sign significantly determines the system evolution. Let us consider the second derivative of the clearly positive R^2

$$R^2 = \frac{\omega''}{2} \int r^2(|A|^2 + |B|^2)\, d\boldsymbol{r} > 0 \,. \tag{8.4.14}$$

Direct calculation with the help of (8.4.1) where (with respect to the parameter $\sqrt{SA_0^2/\omega} \ll 1$) the second derivatives with respect to z can be neglected shows (see Sec. 1.5.4) that $d^2R^2/dt^2 = 2I$. Thus,

$$R(t) = It^2 + 2\alpha t + \beta \,, \tag{8.4.15}$$

where α and β are the constant integrations. Clearly, over a finite time $R^2(t)$ becomes negative when $I < 0$; this fact contradicts (8.4.14). This means that the solution of (8.4.1) "breaks" over the finite time.

Let us study this phenomenon in more detail. To this end, within the frame of the two-dimensional (8.4.4) (where $A(x,y) = B(x,y)$) let us compute the time evolution of the axially symmetrical initial distribution

$$A(\boldsymbol{r},0) = A_0[1 - K(a-r)\exp(-2r^2/\sqrt{\pi}a^2)] \,, \tag{8.4.16}$$

simulating the local increase of the amplitude spontaneously arising during the turbulent motion. It would be natural to select a quarter of the length of the envelope corresponding to the maximum increment as a characteristic length a where $A(r,0) - A_0$ decreases to zero. It gives the estimate

$$a^2 = \pi^2 S^2 \omega'' / \sqrt{(4S+T)^2(h^2V^2 - \gamma^2)} \,. \tag{8.4.17}$$

Figures 8.10, 11 show the results of the computer simulation [8.43]: the evolution of the amplitude $|A(0,t)|$ and of the phase $\Psi(0,t)$ in the center of the packet (Fig 8.10), amplitude distribution $|A(\boldsymbol{r},t)|$ for some characteristic times (Fig. 8.11). Clearly, there is some "critical" modulation depth K_c, such that at $K > K_c$ the packet collapses over the finite time whereas the amplitude in the center increases indefinitely. The critical values of K_c are given in Table 8.2.

Table 8.2. Dependence of critical initial amplitude K_c on the pumping amplitude: $K_1 < K_c < K_2$ (for $K = K_1$ the packet still spreads, whereas for $K = K_2$ it collapses)

$\frac{hV}{\gamma} - 1$	K_1	K_2	$\frac{hV}{\gamma} - 1$	K_1	K_2
10^{-3}	23.0	24.0	1	3.0	3.1
10^{-2}	10.5	11.0	2	2.6	2.7
10^{-1}	5.4	5.5	3	–	0.5
0.4	3.4	3.5			

It can be seen that at $hV - \gamma \ll \gamma$ the critical amplitude $K_c \gg 1$. To understand this fact, note that the phase $\Psi(\boldsymbol{r},t)$ near the focus $r = 0$ of

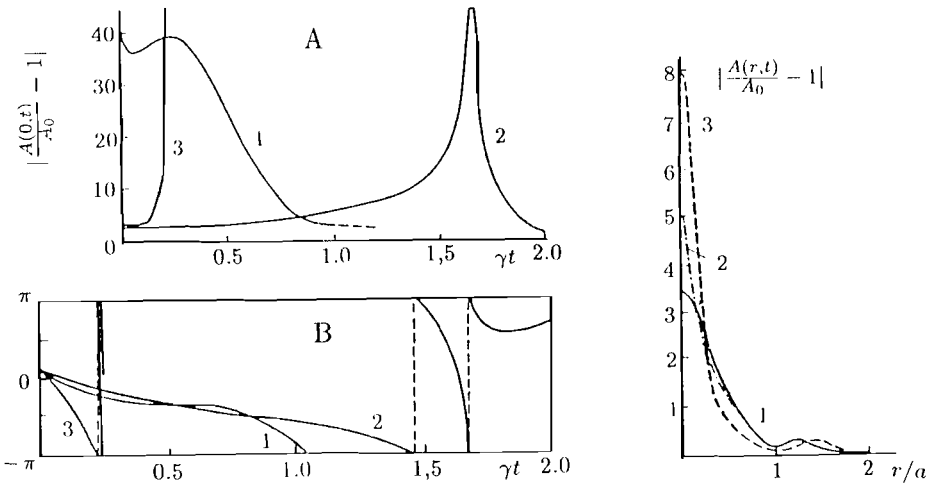

Fig. 8.10. (left) Evolution of the amplitude $A(0,t)$ (A) and phase $\Psi(0,t)$ (B) at the center of a packet for $hV = 2\gamma$, $T = -S > 0$. Curves 1, 2 and 3 correspond to $k = 2.3$ and 3.5, respectively. For the sake of clarity the vertical scale for curve 3A is increased by a factor of 20

Fig. 8.11. (right) Distribution $A(r,t)$, for $hV = 2\gamma$, $T = -S > 0$, $k = 3.5$. Curves 1, 2 and 3 correspond to $\gamma t = 0.05$, 0.125 and 0.2, respectively; $a = 0.8\sqrt{\omega''/\gamma}$

the collapsing packet increases monotonically. This was analytically shown in [8.44] and is clear from Fig. 8.11 at $t > 0.2$. The rotation of the packet phase with respect to the pumping phase leads to the fact that the energy flux to the vicinity of the focus stops; therefore for the collapse the value SA^2 must be at least of the order γ, which significantly exceeds the mean level of turbulence $SA_0^2 \simeq \sqrt{h^2V^2 - \gamma^2}$ in the range $hV - \gamma \ll \gamma$. This result ($(K_c \gg 1$ at $hV - \gamma \ll \gamma)$ is weakly dependent on the choice of the initial distribution phase.

8.4.5 Soliton Mechanism of Amplitude Limitation

As already noted the depth of the amplitude modulation in the turbulent motion is of the order unity, and therefore the probability of formation of solitons with the amplitude significantly exceeding A_0, is exponentially small. This implies (see Table 8.2) that slightly above the threshold there $(hV - \gamma \leq \gamma)$ is almost no soliton collapse. It is clear from Fig. 8.10 that the solitons with the amplitude $1 < K < K_c$ are dispersed. With increasing h the critical value K_c decreases and there is a characteristic amplitude h_c at which $K_c \simeq 1$. Note that the kind of initial distribution (8.4.16) is to a large extent arbitrary, and afterwards under amplitude h_c we shall understand such value of the pumping amplitude above which practically any area with the characteristic diameter $1/\kappa_0$ is covered during the collapse. As is seen

from Fig. 8.12 ($hV = 4\gamma$) for the initial packet with small $K < 1$ as a result of parametric instability the amplitude in the central area increases with the characteristic increment of the order of hV up to the values exceeding unity, after which a quick collapse takes place. This means that under $h > h_c$ nonlinearity not only fails to hinder the instability development, but, on the contrary, leads to an acceleration of the increase and the collapsing of the packet.

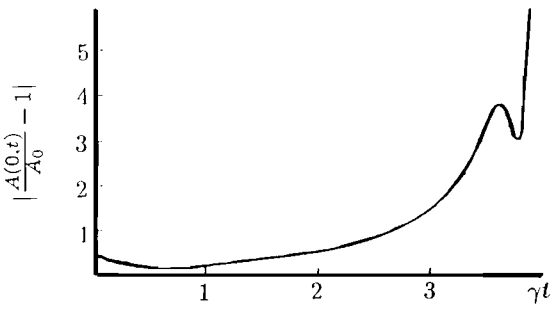

Fig. 8.12. Evolution of $A(0,t)$ at the center of a packet for $hV = 4\gamma$, $T = -S$

Let us consider the phenomena occurring at $h > h_c$. Evidently on studying the evolution of the collapsing soliton the influence of the pumping and damping can be neglected. Equation (8.4.4) in this case is transformed to the nonlinear parabolic equation. The properties of such equations have been studied in detail in connection with the problem of the light self-focusing. As shown in [8.40], the amplitude in the soliton center rapidly increases in time: $A(0,t) \sim (t - t_0)^{-2/3}$. At the same time its radius decreases so that the process of collapse entraps the strictly definite amount of energy

$$I_c = \omega \int |A|^2 \, d\boldsymbol{r} = 1.86\,\omega''\omega/|2S + T| \; . \tag{8.4.18}$$

When the wave amplitude in the collapsing soliton is large enough the nonlinear damping which leads to the fast damping of the soliton energy becomes essential. The effective nonlinear damping can be estimated as $\gamma_{NL} \sim I_c\kappa_0^2/\tau\omega A_0^2 \sim 1/\tau$, where τ is the time between two successive collapses in the area of the size κ_0^2. According to the dimensional estimation $\tau \sim 1/hV$ at $h > h_c$. Taking into account this mechanism of energy dissipation leads to the fact that the mean amplitude of the turbulent pulsations $\langle A \rangle$ becomes less than A_0, and the susceptibility χ'' with the increasing amplitude h does not decrease but reaches the plateau whose order of magnitude coincides with the maximum χ''.

A promising method of experimental research of the strong soliton turbulence of parametrically excited spin waves is the measurement of the spectral density of the electro-magnetic irradiation of the ferromagnet at the frequencies close to the pumping frequency ω_p. At $h < h_c$ when the collapses are rare the spectral density of the noise $(h^2)_\omega$ is close to the Gaussian

with the width $|\omega - \omega_p| \sim \gamma\sqrt{p-1}$. At $h > h_c$ the significant contribution to irradiation is made by the collapsing solitons where the phase of the pair $\Psi(\boldsymbol{r}, t)$ breaks away from the pumping phase and begins to rotate quickly by the law $\Psi(t) \sim (t - t_c)^{-1/3}$ (see [8.41]). The time of breaking away of the phase and several first turns are distinct in Fig. 8.11.

The fast rotation of the phase leads to the significant broadening of the irradiation spectrum $(h^2)_\omega$ which can be used in recording the collapses. By making use of [8.44] we can show that $(h^2)_\omega \sim (\omega - \omega_p)^{-7/4}$. Non-linear damping limiting the amplitude in the collapse $A < A_{max}$ must cut the irradiation at the frequency $SA_{max}^2 \sim |\omega_{max} - \omega_p|$.